J Appl Electrochem (2013) 43:1145–1161
DOI 10.1007/s10800-013-0598-2

RESEARCH ARTICLE

Experimental investigation of two-phase electrolysis processes: comparison with or without gravity

Zine Derhoumi · Philippe Mandin · Hervé Roustan · Rolf Wüthrich

Received: 29 April 2013 / Accepted: 3 August 2013 / Published online: 29 August 2013

Abstract During two-phase electrolysis, bubble production occurs at one or two electrodes. This yields a large change for the electrolyser electrical and hydrodynamic properties. Under normal Earth gravity, the bubble production at the electrodes induces a macro-convection in the electrolyser. This leads to a modified local current density distribution at the electrodes. When gravity is avoided, bubbles are no longer subject to buoyancy forces and to the induced natural flow friction forces. Electrolysis was performed using a potentiostat, and gas bubble evolution was observed with cameras. Quantitative evolution laws for the electrochemical cell voltage, bubble diameter and population during two-phase electrolysis are established in function of the current density and gravity variation.

Keywords Two-phase electrolysis · Bubbles · Electrochemical · Processes · Gravity

List of symbols

δ	Electrode two-phase boundary layer thickness (m)
d	Average bubble diameter (mm)
Δd	Standard deviation of bubble diameter (mm)
E°	Thermodynamical standard RedOx potential (V)
ε	Gas bubble void fraction (−)
G	Normal Earth gravity acceleration = 9.81 m s^{-2}
j	Applied current density (A m^{-2})
μ	Dynamic viscosity (Pa s)
N	Bubble population (bubbles cm^{-2})
n	Bubble number (−)
P	Pressure level
P°	Atmospheric pressure condition (1.013×10^5 Pa)
ρ	Density (kg m^{-3})
S	Surface area (m^2)
σ	Electrical conductivity (S m^{-1})
T	Temperature in interval (about 295 K)
t	time (s)
θ	Electrode bubble surface screening (−)
XG	Dimensionless gravity = −1 or +1, respectively, for 1G or 0G level
Xj	Dimensionless current density = −1 or +1 respectively for min or Max j

Subscript

O_2	Oxygen at anode
H_2	Hydrogen at cathode
P	Pixel
ini	Initial
end	Final, generally @ $t = 20$ s
tot	Total
0	Initial or bulk liquid electrolyte condition

1 Highlights

Cell voltages and overvoltages occurring during water electrolysis have been measured and are related with the two-phase boundary layer structure in terms of bubbles

Philippe Mandin is ISE and ECS member.

Z. Derhoumi · P. Mandin (✉)
Centre de recherche rue de Saint-Maudé, LIMatB EA4250, Université de Bretagne Sud, 56100 Lorient, France
e-mail: philippe.mandin@univ-ubs.fr

H. Roustan
Rio Tinto-Alcan – Centre de Recherche de Voreppe, 725 rue Aristide Bergès, BP 27, 38341 Voreppe Cedex, France

R. Wüthrich
Department of Mechanical and Industrial Engineering, Concordia University, 1455 de Maisonneuve Blvd. West, Montreal, QC H3G 1M8, Canada

diameter and population. Sensitivity analysis with two explored parameters, current density j and gravity G, is also performed. This second parameter is not yet extensively explored in the literature. This paper gives quantitative input and output information for two-phase electrolysis multi-physics multi-scale modelling. The quantitative link between two-phase boundary layer structure and overvoltage is presented. The variation of gravity helps in estimating the bubble accumulation consequences during two-phase electrolysis.

2 Introduction

The present study deals with the evolution of the electrode bubble boundary layers produced during two-phase electrolysis of an aqueous solution and its effect on the cell voltage. The goal is to relate the cell overvoltage with the two-phase boundary layer's structure in term of thickness δ (m), bubbles diameter d (mm), standard deviation/diameter dispersion Δd (mm), population N (bubbles cm^{-2}) and gas void fraction ε (−) at both electrodes (Fig. 1). Experiments in different conditions of current density j (A m^{-2}) and gravity G (normal Earth gravity $1G = 9.81$ m s^{-2} and reduced microgravity $0G$) have been performed on a simple electrochemical cell.

A scheme of the experimental strategy is presented in Fig. 1b.

During the present electrolysis, gas production occurs at both electrodes (anode, gold, and cathode, copper) according to reactions (1)–(3):

$$\text{Anode: } 2H_2O \rightleftharpoons 4H^+ + 4e^- + O_2 \quad E^0(O_2/H_2O) = +1.23\ \text{V} \tag{1}$$

$$\text{Cathode: } Cu^{2+} + 2e \rightleftharpoons Cu \quad E^0(Cu^{2+}/Cu) = +0.34\ \text{V} \tag{2}$$

$$4H^+ + 4e \rightleftharpoons 2H_2 \quad E^0(H^+/H_2) = 0\,\text{V} \tag{3}$$

The anode (gold) oxidation is neglected in the present work.

Few works concerning two-phase electrolysis, from the experimental and modelling point of view, are available in the literature despite several important industrial processes are involved such as hydrogen, fluorine, chlorine

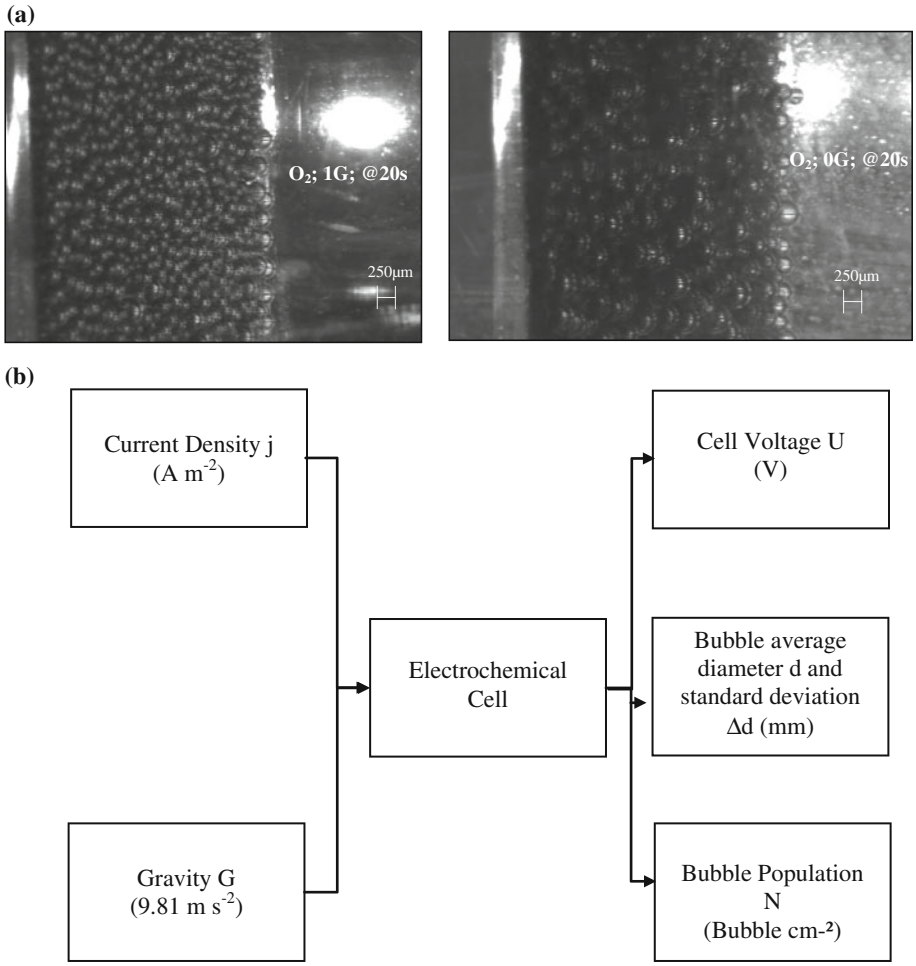

Fig. 1 **a** CCD images of O_2 gas bubbles evolution and two-phase boundary layer at gold anode in ($CuSO_4 + Na_2SO_4$) liquid electrolyte under normal Earth gravity $1G$ and during microgravity flights $0G$, at 20 s after electrolysis starting. **b** Two-phase electrolysis study strategy: explored factors and measured experimental results

or aluminium production. The overpotential due to bubbles is generally described with an added Bruggeman resistance R (Ω) related to an estimated gas void fraction ε ($-$). The challenge is to obtain an accurate estimation of the two-phase boundary layer thickness δ (m) at the electrodes to ensure the correct gas void fraction and resistance estimation. This boundary layer, under Earth conditions (gravity $= 1G = 9.81$ m s^{-2}), yields a vertically dependent gas void fraction strongly coupled with bubble and electrolysis reactor scales. This is the reason why theoretical and experimental studies in the zero gravity condition are of great interest. In fact, these experiments are both difficult and expensive to perform. Matsushima et al. [1, 2] observed oxygen and hydrogen gas evolution on platinum electrodes in alkaline and acid solutions during 8 s in a microgravity environment realized in a drop shaft. They reported that the effect of gravity level is greater in the case of KOH solution than in H_2SO_4 solution. They have also shown that in alkaline solutions, the current density j is much smaller under microgravity than under Earth gravity. Further, the

Table 1 Experimental design and 4 experiments' definition

Exp.	Gravity XG	Current density Xj
1	−	−
2	−	+
3	+	−
4	+	+

When $XG = -1$, $1G = 9.81$ m s^{-2}; when $XG = +1$, $0G = 0$ m s^{-2}; when $Xj = -1$, $j = 96$ A m^{-2}; and when $Xj = +1$, $j = 129$ A m^{-2}

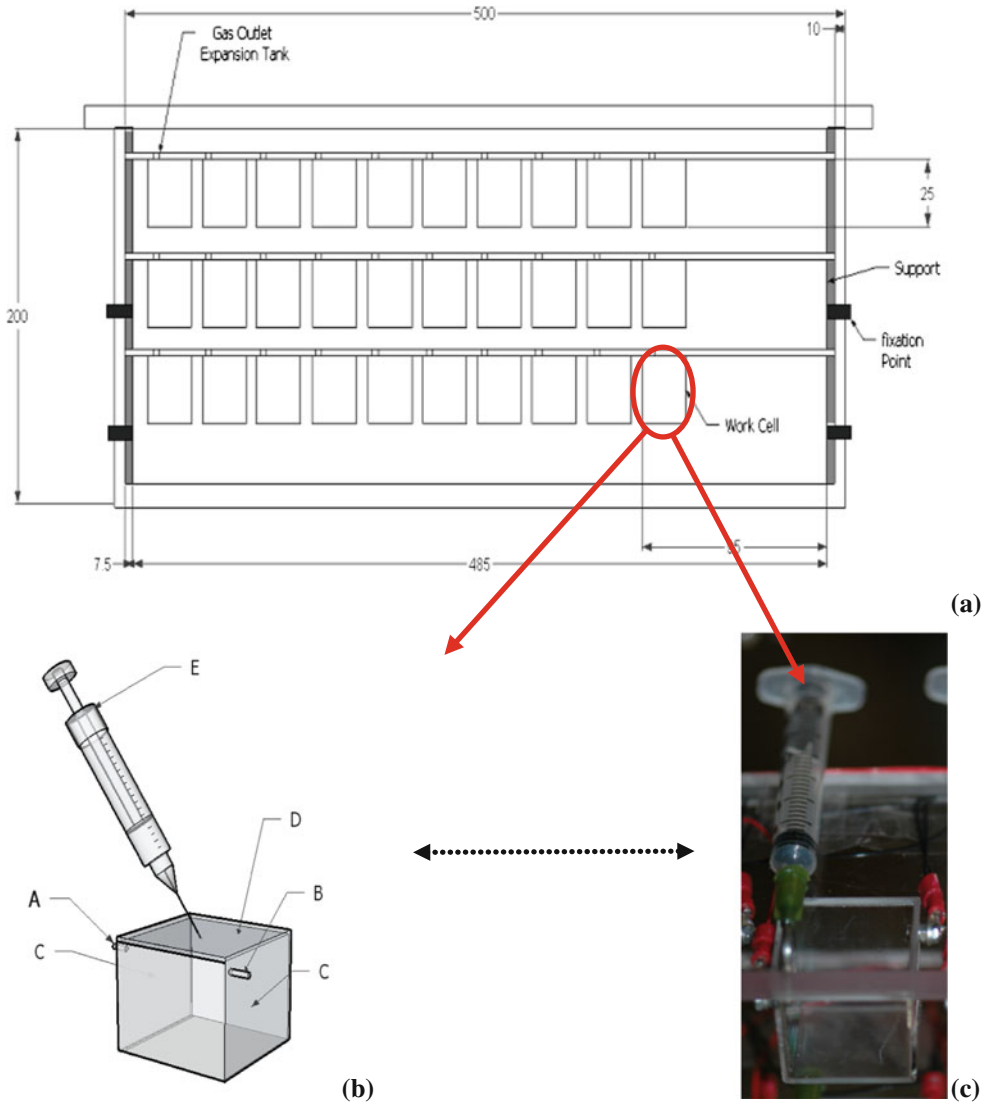

Fig. 2 **a** Schematic 2D general experimental device with the 30 electrochemical cells; **b** Elementary schematic electrochemical cell: *A* Au anode connection; *B* Cu cathode connection; *C* electrodes; *D* PMMA Cell; *E* Syringe; and **c** Elementary electrochemical cell photography

authors showed that the electrical resistance increases under zero gravity due to the formation of a gas bubble layer and an increase in electrode surface coverage by bubbles [1, 2].

Brussieux et al. [3] have performed a study of gas release (hydrogen bubbles) during water electrolysis. The conclusion of this work is in good accord with our previous work [4] and Vogt's theoretical results [5–7]. Vogt et al. [5–7] noted the influence of the flow velocity in a stagnant fluid and forced or gravity-induced fluid flow with speeds ranging from 0.01 to 0.3 m s^{-1}. It was noticed that the gas void fraction ε decreases with increasing flow velocity. Numerical simulations carried out by Mandin et al. [8, 9] have been tried for normal Earth gravity to model the bubble production influence onto the current density j distribution, through a vertical position-dependent gas void fraction ε and electrical conductivity σ (S m^{-1}). This kind of work was completed and validated with the experimental work of Wüthich et al. [10, 11] and Tobias et al. [12]. It has been shown that the two-scale free convections on Earth made a correct primary or secondary two-phase electrolysis modelling difficult. It was therefore decided to perform both experiments under zero and normal gravity condition to obtain accurate quantitative evidence for two-phase electrolysis modelling.

Concerning more specific zero gravity works, a decrease in overall cell performance is also observed for both methanol fuel cells and electrolysis reactor due to gas bubbles enlargement [13]. Kaneko or Guo et al. [14, 15] also investigated water electrolysis under zero gravity condition and found that gas bubbles become larger, whereas current densities decreased in microgravity. Their results allow the hypothesis that during electrolysis, the water species mass transfer to the electrode controls the process. However, under normal Earth gravity conditions, water electrolysis is said to be kinetically limited [15].

From the kinetics point of view, Iwasaki et al. [16] demonstrated the existence of a faster steady state for electrolysis current under normal gravity and free convection than that under pure diffusion zero gravity conditions [16].

More recently, in 2012, Nicolau et al. [17], using the Nasa Boeing for zero gravity experiments, performed ammonia oxidation experiments.

In the present study, experiments in microgravity and in the presence of gravity were conducted according to the experimental design presented in Table 1. The current density j has been chosen around 100 A m^{-2}, which is about ten times smaller than the order of range of the applied current for industrial partners (between 0.1 and 1 A cm^{-2}). These smaller values have been chosen due to aircraft safety constraints and also to organize a modelling strategy from small to large current density values. The second level models a 30 % increase of the applied current density j.

The work was performed for each of these explored inputs for two level values, -1 and $+1$, which are, respectively, the minimal and maximal values. The four performed experiments and the quantitative values for inputs are given in Table 1.

3 Methods

3.1 Electrochemical system

An electrolytic cell (25 mm × 25 mm × 25 mm) as illustrated in Fig. 2b, c was employed. Figure 2a shows the arrangement of the 30 identical electrochemical cells during the $0G$ aircraft experimental conditions. The electrodes had a surface area of 25 mm × 22.6 mm and were made of 0.1-mm metal sheets (Good Fellow®), copper for the cathode and gold for the anode. The two electrodes were attached to the cell walls using a system of double-sided adhesive. The electrical connection is established using two stainless steel screws that are in contact with the two electrodes.

The electrochemical cells were filled with a copper sodium sulphate mixture (Sigma Aldricht® $CuSO_4 + Na_2SO_4$) as an aqueous electrolyte. The electrolyte properties are given in Table 2. Density has been measured using a microbalance. Electrical conductivity has been measured using a C5010 Consort® apparatus. The measured value is in good agreement with the usual given values for such an electrolyte.

Safety constraints within the aircraft require the utilisation of perfectly sealed electrochemical cells. An expansion tank (a 3-mL medical syringe; Fig. 2b and c) has been used to drain the gas produced during electrolysis to avoid pressure increase.

The experiments, performed according to the experimental design presented in Table 1, were performed under a temperature T of about 295 K and a pressure level $P = 1.013$ bar. Each used electrochemical cell, for both $1G$ and $0G$ experiments, was filled with the electrolytic solution 24 h before the actual electrolysis.

3.2 Electrolysis and cell voltage acquisition

Electrolysis and voltage acquisition are performed with a Metrohm-Autolab potentiostat PGSTAT302 N. The NOVA 1.5 software is used with a chronopotentiometry procedure at 100-Hz acquisition frequency. This, usually used on Earth laboratory, apparatus has been utilised for the present exploration of the gravity effect on two-phase electrolysis overvoltages and two-phase boundary layer structure in the $0G$ experiments. Because of this, an approximately 150-kg rack has been developed. The potentiostat and

electrochemical cells have been placed and fixed, according to the mechanical and electrical Novespace® safety standards, in the rack.

3.3 Video acquisition system

Bubble growth at the electrodes' edges and cell boarders as well as the direct 'in front' visualisation of the two-phase layer thickness is impossible due to the screening produced by the bubbles. Therefore, a four-camera configuration (two per electrodes) with a recording angle of about 30° was used.

The gas bubble formation was observed by Giant Dragon CCD and 'general view' CANON cameras. The CCD cameras were connected to a laptop PC via an ethernet connection, whereas the CANON cameras recorded with an internal memory. All cameras were mounted on an aluminium support and observe the electrode surface at a 30° angle with, respectively, 90 fps for the CCD and 60 fps for the CANON cameras.

3.4 Images processing

The VirtuelDub® software was used to analyse the CCD videos and divide them in pictures according the method presented in Ref. [4]. The ImageJ® software was used to analyse individual pictures (Fig. 3). This analysis allows the determination of the bubble diameter distribution (average diameter d and standard deviation Δd) and the bubble population density (bubbles per cm^2) in function of time t.

Table 2 Liquid electrolyte properties at $T = 298$ K

Density, ρ_0 (kg m^{-3})	Conductivity, σ_0 (S m^{-1})	$CuSO_4$ concentration (mol L^{-1})	$CuSO_4$ concentration (g L^{-1})	Na_2SO_4 concentration (mol L^{-1})	Na_2SO_4 concentration (g L^{-1})
$1.05 \times 10^{+3}$	3.42×10^{0}	5.3×10^{-2}	$1.32 \times 10^{+1}$	3.89×10^{-1}	$5.10 \times 10^{+1}$

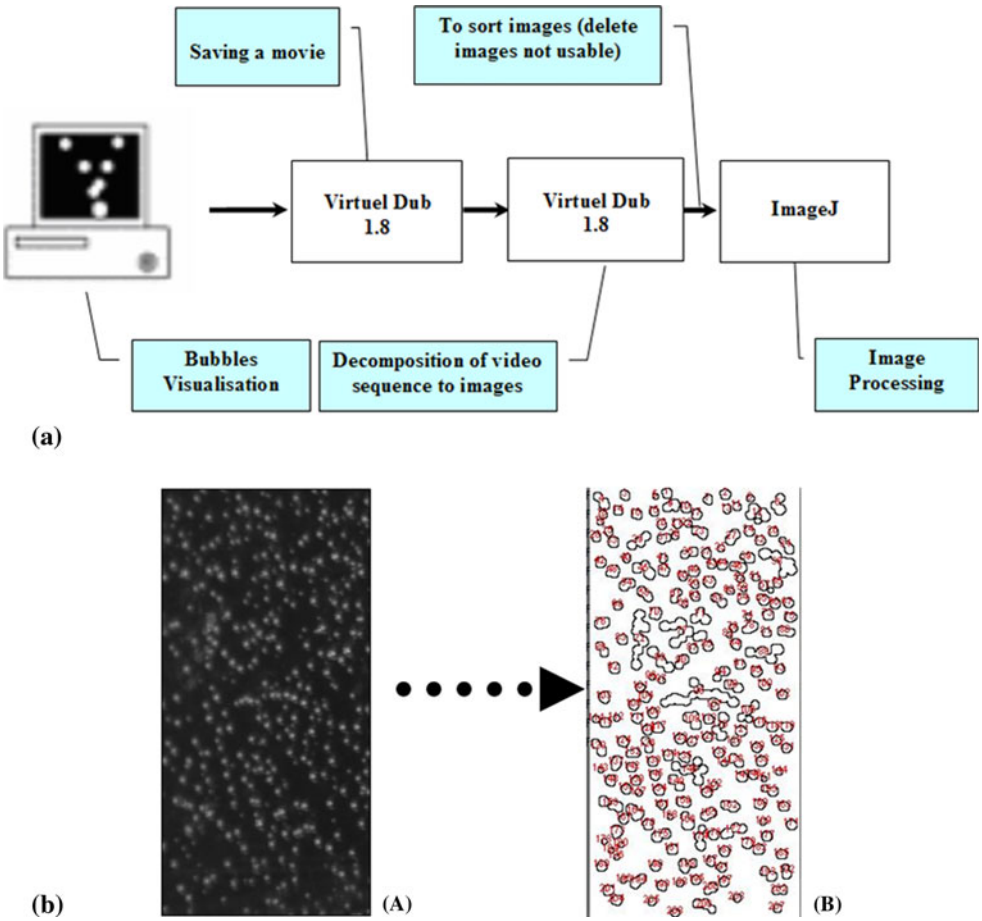

Fig. 3 **a** Video processing strategy; **b** O_2 Image thresholding process: (*A*) image extract from CCD video; (*B*) processed image with ImageJ® software

Using the thresholding function pixels with brightness values between a minimum (about 0.5) and a maximum (about 1) values are detected and marked (Fig. 3B). The maximum and minimum values define the threshold interval on which the definition of one actual particle (bubble) is assumed. According to Fig. 3, the strategy for image processing, for a given image domain with area S, n bubbles are detected with area S_{tot}.

The single bubble average area and diameter is calculated according

$$S_{\text{bubble}} = \frac{S_{\text{tot}}}{n} \tag{4}$$

$$d = \sqrt{\frac{4S_{bubble}}{\pi}} \tag{4'}$$

An estimation of the bubble electrode surface screening θ is

$$\theta = {}^{S_{\text{tot}}}/_{S} \tag{5}$$

This is an overestimation because the contact angle of the bubble with the electrode surface must be 90° which is not always the case.

In the used configuration 1 pixel = 2.6 x 2.6 × 10^{-2} mm.

In order this method to be accurate one bubble must be made of a large number of pixels. The estimation of the average minimal number of pixels per bubble can be done as follows.

The number n_{P} of pixels per average bubble is given by:

$$n_{\text{P}} = \frac{1 \text{ average bubble area}}{1 \text{ pixel area}} \frac{\frac{S_{\text{tot}}}{n}}{1 \text{ pixel area}} \tag{6}$$

The diameter estimation according to this method, when a threshold min value is chosen, is estimated equal to one pixel length divided by one average diameter. The minimal pixel numbers n_{p} to describe one average bubble is about 80. This shows the accuracy of the image processing method used in this study.

3.5 0*G* experiments and parabolic flight

Experiments in 0*G* in microgravity were conducted in the NOVESPACE® Airbus A300 aircraft.

The allocated space allowed the use of three shelves disposed in a double containment. Ten cells per shelf were mounted. The cells are arranged in three rows of ten as shown in Fig. 2. The cells are controlled by a PLC (control box) and allow the switching from a cell to another to perform 30 different electrolysis experiments successively.

The aircraft climbs with a pitch angle of 47°. The sensation of weightlessness is achieved by reducing thrust and lowering the nose to maintain a zero-lift angle of attack. Weightlessness begins whilst ascending and lasts all the way 'up-and-over the hump', until the craft reaches a declined angle of 30° (Fig. 4).

Temperature and pressure levels during experiments in the aircraft are measured in the same time as acceleration levels. This is mainly to ensure the equivalence with 'on Earth' conditions, experiments 1 and 2.

The pressure P–$P°$ (Fig. 5a) inside the box was measured by JUMO dTRANS p30 pressure transducers (0–1.6 bar). The pressure level inside the insulated double containment, though the aircraft pressure was about 0.8 Bars, was found quite constant at atmospheric condition $P° = 1.013$ bar.

A K-type thermocouple was placed inside the box near the cells in order to acquire the evolution of the local temperature T (K) with a MicroDAQ-73T USB capture card (Fig. 5b).

The parabola quality is strongly related to the maximal acceleration measured during zero gravity periods. This maximal acceleration should be in the range of $-0.05G$ to $+0.05G$ to ensure 'a good parabola' (Fig. 5c).

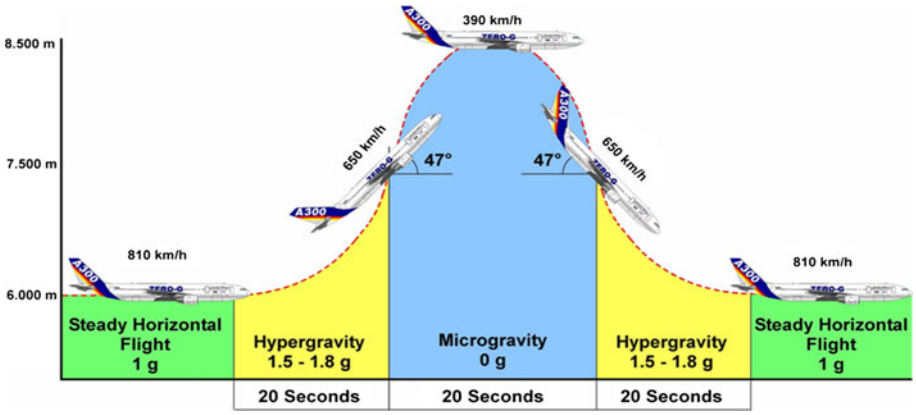

Fig. 4 0*G* parabolic flight

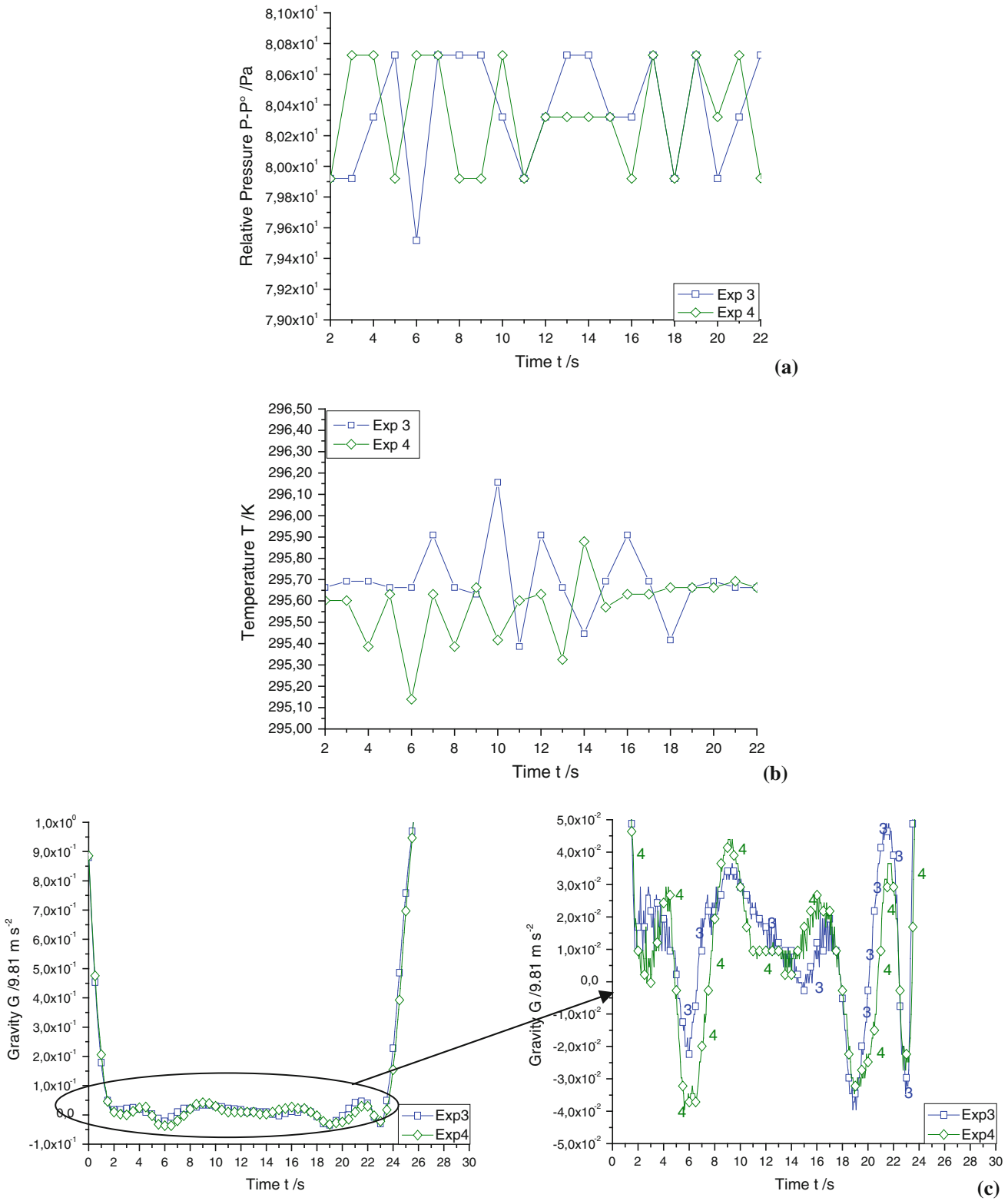

Fig. 5 **a** Pressure evolution. **b** Temperature evolution. **c** 0*G* quality in the aircraft

4 Results

4.1 Cell voltages evolution

Figure 1b gives input variables which are the applied electrical current density j (A m^{-2}) and the imposed acceleration/gravity G (m s^{-2}).

The outputs are the final cell terminal voltage U (V) (and also the bubble overvoltage), the bubble diameter d(m) and the bubble population density N (bubbles cm^{-2}). Other input parameters of the experiments, such as temperature (T in [295; 296] K), ambient pressure level ($P^{\circ} = 1.013 \times 10^5$ Pa) and chemical composition are kept constant for all the experiments in the present work.

In Fig. 6, the cell voltage time evolution shows an increase for all four presented experiments.

Figure 6 and Table 3 show that for both, Earth and zero gravity experiments, the cell voltage increases with applied current density. More interesting is the cell voltage behaviour with the gravity for a given applied current density j. The final cell voltage is smaller at zero gravity than at Earth gravity.

In Fig. 6, different characteristic time periods are defined:

1. Bubble nucleation; first O_2 and then H_2;
2. visible bubble onset on the CCD camera; first O_2 and then H_2;
3. and finally the cell voltage stabilization period.

This third part is absent in experiments 1 and 2 due to insufficient time for electrode activation and product species steady accumulation.

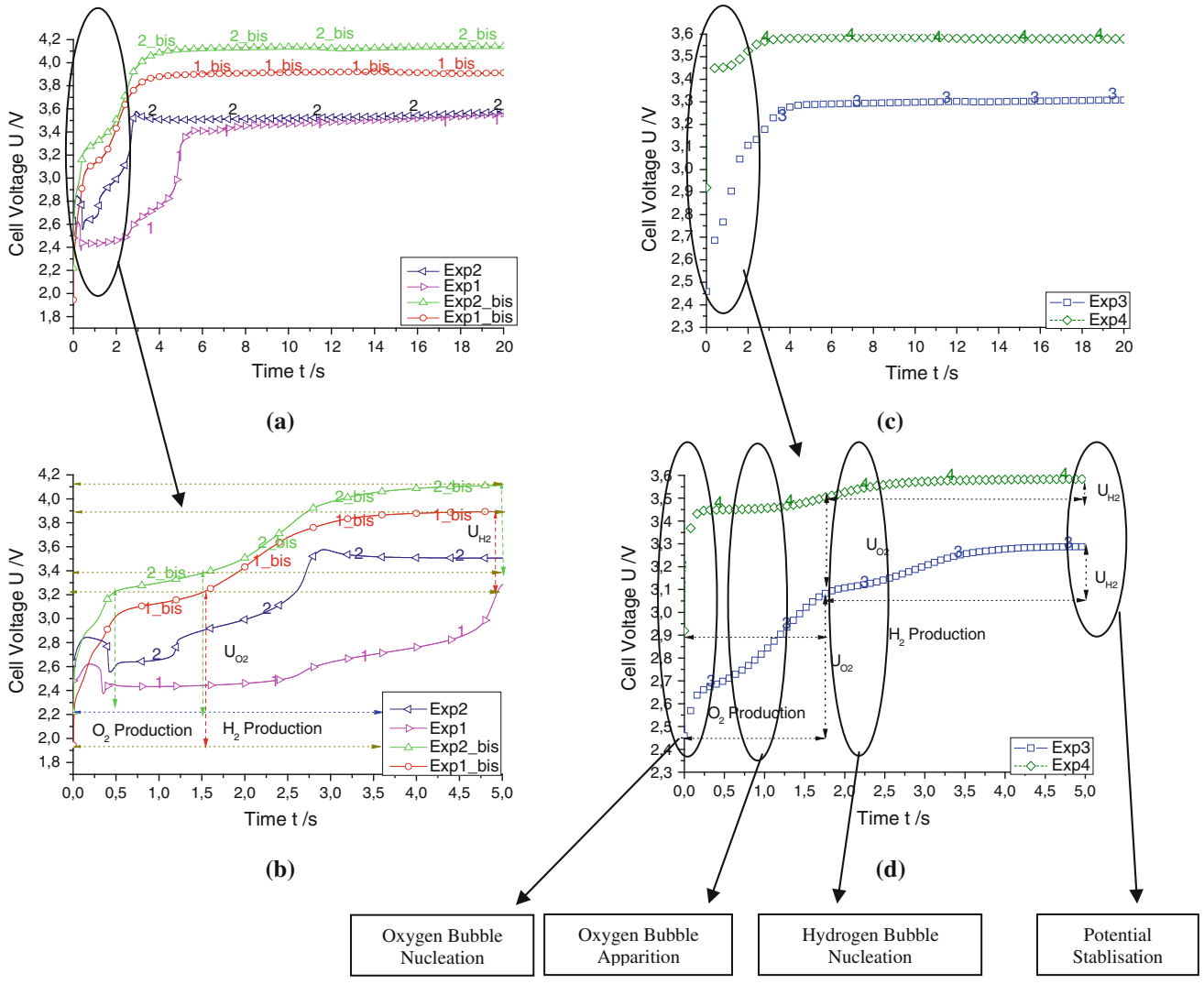

Fig. 6 Cell voltage U (V) evolution with time t (s) for the 4 defined experiments—**a**: Gravity 1G; **b**: 1G zoom from t = 0–5 s; **c** Gravity 0G; **d** 0G zoom from t = 0–5 s

Non-reproducible $1G$ experiment results, in term of initial and final cell voltage, are observed at the initial times of the electrolysis. This is because electrodes have not worked long enough and the produced species concentration at the electrodes is not sufficient.

This is the reason why two additional tests, called 'bis' and 'ter', have been performed to show that a second $1G$ experiment is necessary just after the first one in order to obtain reproducible results, particularly with new, never used, electrochemical cells. When the third experiment 'ter' was performed, it leads to identical results to the second experiment 'bis'. Consequently, each $1G$ experiment has been performed only two times.

It is more challenging to perform experiments at $0G$ than under $1G$ condition. It was decided to use three dedicated parabolic experiments to discuss the problem of the initial voltage. In Table 4, it is shown that sufficient electrode activation and product species concentration are obtained during the first electrolysis concerning the final cell voltage (last column) but not the initial cell voltage (first column). The experiment under $0G$ has been performed three successive times under condition 3. The experiment in condition 4, under $0G$, has been performed two times and shows the same conclusion as experiment 3.

Figure 6 shows six experimental voltage evolutions. Each $1G$ experiment has been performed two times. Further shown are experiment 1 and 1bis, and 2 and 2bis (Fig. 6a, b). As can be seen with experiments 1 and 2, under $1G$ condition during 40 s electrolysis, a steady state is not reached. This is because there is not enough electrode activation and product accumulation at the electrodes due to the convective flow. With a second electrolysis (experiments 1bis and 2bis, Fig. 6a, b), we can observe that the steady state is reached within only about 5 s and product species concentration at the electrodes is sufficient.

This behaviour is also observed with $0G$ experiments 3 and 4, but without the need of 'bis' experiments concerning the final cell voltage. In Fig. 6c and d, it can be observed that the steady state is reached in about 5 s.

In the 'initial cell voltage' row (Tables 3, 4), it can be observed that, in the absence of produced species, the initial cell voltages are larger for experiments 1, 2 at $1G$ and also 3, 4 at $0G$ than for experiments 1bis, 2bis and 3bis, 4bis. The consequence is shown in Table 3: the initial cell voltage for a given electrochemical reaction set is much larger than the voltage necessary after few electrolysis experiments. This means that electrochemical reactions are easier initially to proceed than after electrode activation and product species accumulation at the electrodes. This is also what the first row shows in Table 4 with a continuous decrease of the initial cell voltage at $0G$. Concerning the final cell voltage, it can be considered, using Table 4, that they are identical at three consecutives electrolysis experiments.

In our opinion, these initial cell voltages can be associated with the cell voltage without any bubbles at both electrodes, but with electrode activation and product species at the electrode vicinity. The two electrochemical reactions occur at the electrodes, but the produced species are in dissolved form, not yet in form of bubbles.

The reasons are not available in the current literature. What is clear is that the initial voltage (Tables 3, 4, first column) decreases with the number of successive experiments, whereas the final voltage follows the inverse trend (second column). In our opinion, there is a start-up, an activation phenomenon, which explains the initial voltage trend. After the very first electrolysis, the electrode is ready to perform the reaction due to activation sites. Concerning the final cell voltage, at the end of the first electrolysis, the voltage is smaller than after the second electrolysis. But, after the third electrolysis, there is no more any change observed. This trend is more important under $1G$ than under $0G$ (see Table 4). It must be due to the induced flow and dissolved species accumulation. Under $0G$, there is no change.

In fact, more produced bubbles do not yield to a larger ohmic resistance. It depends of the bubbles behaviour. What is interesting to see is that the H_2 voltage drop

Table 3 Cell voltage evolution under $1G$ and $0G$ condition (compare with Fig. 6)

Exp.	Initial cell voltage, V U_{ini}	Terminal cell voltage, V U_{end}	Time for bubbles appearance, s		Voltage drops, V		Drops sum V
			t_{O_2}	t_{H_2}	ΔU_{O_2}	ΔU_{H_2}	ΔU
1	2.48	3.56	5×10^{-1}	2.25	-1×10^{-1}	1.09	9.9×10^{-1}
2	2.63	3.58	5×10^{-1}	1.25	2×10^{-1}	7.5×10^{-1}	9.5×10^{-1}
1bis	1.94	3.91	5×10^{-1}	1.5	1.28	6.9×10^{-1}	1.97
2bis	2.21	4.14	5×10^{-1}	1.5	1.16	7.7×10^{-1}	1.93
3	2.45	3.35	1.2×10^{-1}	1.75	6×10^{-1}	8.1×10^{-1}	1.41
4	2.91	3.58	1.2×10^{-1}	1.75	5.9×10^{-1}	7.8×10^{-1}	1.37

remains about constant from 1G to 0G, due to the existence of a horizontal H_2 motion under 0G which leads to no H_2 bubble accumulation at the cathode with or without gravity and induced flow. The behaviour of O_2 bubbles is different: There are fewer bubbles seen at the anode, certainly due to multi-generation layers formation. The two-phase O_2 layer must be of larger thickness, but smaller gas void fraction under 0G. There is likely some percolation or 'electrical bridge' effect which enhances the apparent electrical conductivity through the layer. One must also keep in mind that the bubble motion is also a mass transfer enhancement source.

Due to induced flow friction and buoyancy, the bubble attachment and electrode screening decrease and yield to a smaller cell voltage. However, under 0G, in the present work, we observe a cell voltage decrease (e.g. from exp1/exp1bis to exp3). These results are reproducible as shown in Table 4 which shows that experiment 3 has been performed three successive times and yields the same result every time. One explanation might be obtained considering that the bubble population (Table 6) is obtained 'on the top' and does not give any information concerning the bubble layer thickness. Table 6 shows that O_2 bubbles are less numerous under 0G. But, the thickness must be larger because the gas production is the same. The resulting gas void fraction is smaller and as the resulting voltage drop is smaller too.

Quantitative calculations are necessary for the following reasons:

1. Usually, the larger the current density, the larger the attached bubbles population is.
2. But, when many bubbles are produced per unit time, the flux is also important. The induced flow is increased and the friction too. Because of this, it is possible to imagine that large current density yields smaller bubble populations hardly detectable with the used CCD camera. Caution is required as the bubble population N is not counted for all the bubbles attached at the electrode (no view in the two-phase layer thickness), and there are also many 'free' bubbles which are also not seen in the CCD recording.
3. Large current density means large bubble production per unit time: among them, few stay attached at the electrode; many leave the electrode vicinity because of friction and buoyancy forces.

This is of interest in the present quantitative study to help multi-physics modelling for two-phase electrolysis.

Eventually, gas bubbles appear, once the produced species concentration reaches supersaturation locally. In the present paper, it is supposed that the two bubble layers lead to an overvoltage, which is measured between the initial and the final cell voltage. According with the associated videos, the oxygen bubble nucleation and growth occur before the hydrogen one. It is proposed to attribute the two consecutive voltage drops to, firstly, the oxygen bubbles and, secondly, the hydrogen bubbles.

What is important is the voltage drop due to both O_2 and H_2 bubble layers and their sum (last row of Table 3). These drop sums are independent of the applied current density j, but they decrease with zero gravity.

This fact shows the importance of the two-phase boundary layer structure upon the cell voltage for a given applied current density. This is the reason why we want to identify the relation between these near electrode bubble layers and the overvoltage.

After this qualitative and quantitative result presentation, the aim of the present work is to establish a synthetic quantitative formulation of the two explored factors upon the cell voltage increase. This is the reason why multi-linear interpolation has been performed between cell voltage and the two input parameters, current density j and gravity G. This experimentally obtained formulation will be, in further work, used to validate numerical two-phase electrolysis multi-physics models.

According to Table 3, O_2 bubbles first appear and are supposed to be responsible for the first cell voltage increase, called ΔU_{O_2}. The associated values are given in Table 3. After bi-linear interpolation using a H_4 Hadamard matrix, the cell voltage drop associated with O_2 bubbles is

$$\Delta U_{O_2} = 9.1 \times 10^{-1} - 3 \times 10^{-2} Xj - 3.1 \times 10^{-1} XG + 3 \times 10^{-2} Xj\,XG \quad (7)$$

with

$Xj = -1$ and $+1$ when the actual current density value is $j = 96$ and 129 A m^{-2}, respectively, $XG = -1$ and $+1$ when respectively the actual gravity value is $G = 9.81$ and 0 m s^{-2}, respectively.

The writing in the dimensionless form for explored parameters j and G allows the comparison between the two input factors and their interaction $Xj\,XG$. It appears that for a 30 % current density increase, the overvoltage decrease is 6×10^{-2} V, which is about 7 % of the O_2 bubble-

Table 4 Cell voltage reproducibility in Microgravity (Exp 3) and Earth gravity (Exp 4)

	Initial cell voltage U_{ini}/V	Terminal cell voltage @ $t = 20$ s U_{end}/V
Exp 3	2.67	3.33
Exp 3bis	1.93	3.36
Exp 3tre	1.91	3.4
Exp 4	3.14	3.65
Exp 4bis	2.34	3.68

associated overvoltage. Concerning the gravity G, the absence of the buoyancy forces yields an overvoltage decrease of 6.2×10^{-1} V, which is about 67 %. One can understand the importance of the gravity G upon the overvoltage. In the same range, a relatively small influence of the current density appears. This influence is non-linear. It should be noticed here that the interpolation with the two explored factors j and G is not perfectly linear: an experimental dispersion or an interaction should mostly be taken into account which is the same order of range, 3×10^{-2} V, as the current density effect, but one order of range smaller than the gravity effect. This represents about 3 % of the average O_2-associated overvoltage.

The observation that this overvoltage decrease with increasing current density is unusual. It is important to discuss the result in the light of reproducibility tests. One experiment has been performed three times in identical conditions and yields a standard deviation upon the cell voltage of about 3×10^{-2} V. The applied current density has a negligible influence upon these two cell voltage increases associated with O_2 and H_2 bubbles. The voltage drop due to the two-phase layer is slightly affected by the current density at 1 G. At 0G, the current density influence is more important especially upon the H_2 layer.

According Table 3, H_2 bubbles appear after O_2 ones and yield the second cell voltage increase, called ΔU_{H_2}. After

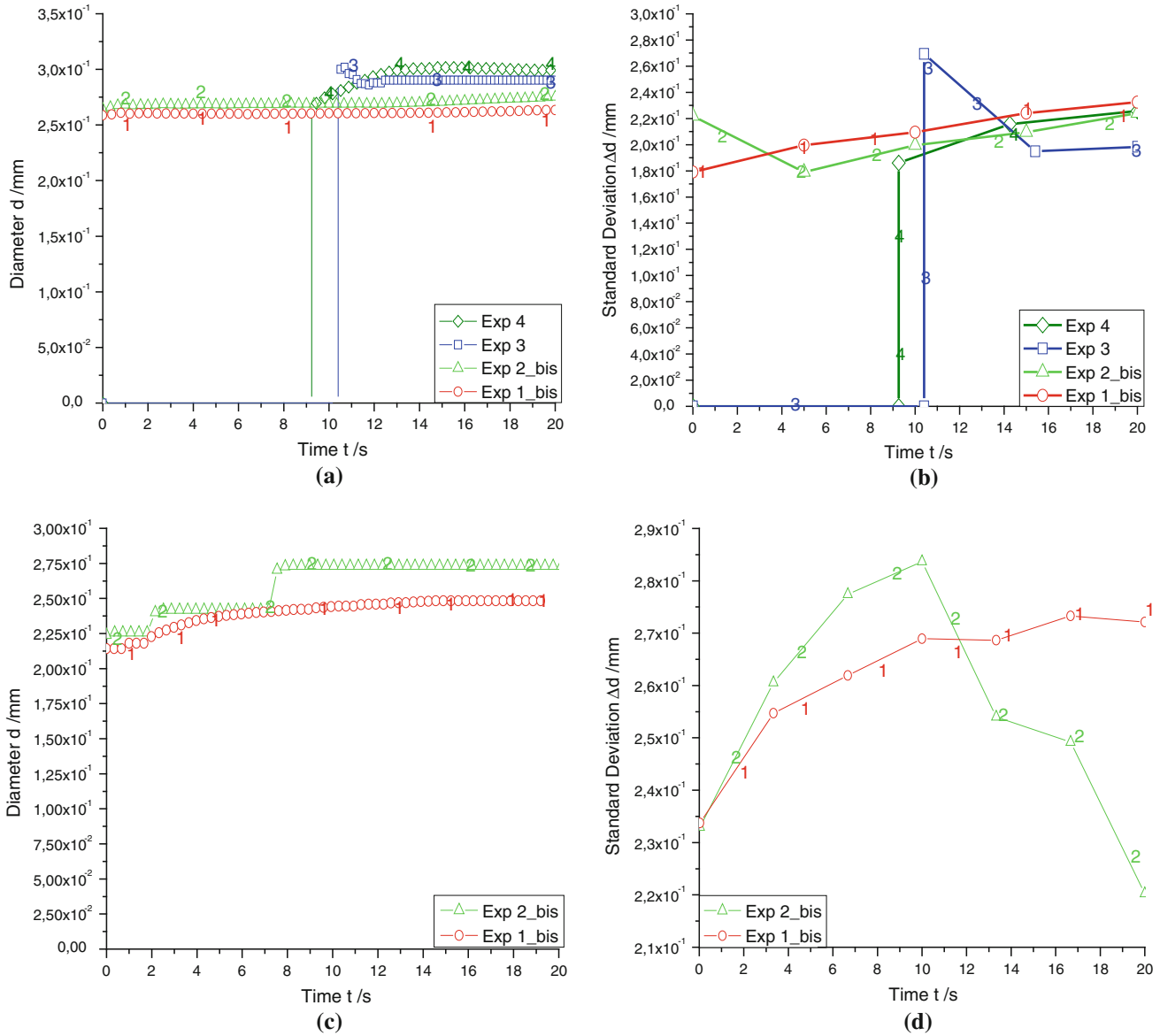

Fig. 7 O_2 and H_2 bubble diameter evolution with time for the 4 defined experiments. **a** Average diameter d_{O_2} (mm). **b** Standard deviation Δd_{O_2} (mm). **c** Average diameter d_{H_2} (mm). **d** Standard deviation Δd_{H_2} (mm)

Table 5 Terminal O_2 and H_2 average diameter d (mm) and standard deviation Δd (mm)

Exp.	d_{O_2}/mm @ $t = 20$ s	Δd_{O_2}/mm @ $t = 20$ s	d_{H_2}/mm @ $t = 20$ s	Δd_{H_2}/mm@ $t = 20$ s
1	2.6×10^{-1}	2.2×10^{-1}	2.4×10^{-1}	2.7×10^{-1}
2	2.7×10^{-1}	2.1×10^{-1}	2.7×10^{-1}	2.2×10^{-1}
3	2.9×10^{-1}	2.0×10^{-1}	×	×
4	3×10^{-1}	2.2×10^{-1}	×	×

bi-linear interpolation, the cell voltage drop associated with H_2 bubbles is

$$\Delta U_{H_2} = 7.62 \times 10^{-1} + 1.25 \times 10^{-2} Xj + 3.25 \times 10^{-2} XG - 2.75 \times 10^{-2} Xj\, XG \quad (8)$$

For a 30 % current density increase, the overvoltage increases by 2.5×10^{-2} V, which is about 3 % the H_2 bubble-associated overvoltage. Concerning the gravity, the disappearance of the buoyancy forces yields an overvoltage increase of 6.5×10^{-2} V, which is about 9 %. It should be noticed here that the interpolation with the two explored factors j and G is not linear: an experimental dispersion or an interaction should mostly be taken into account which is the double order of range, 5.5×10^{-2} V, compared to the current density effect, but one quarter smaller than the gravity effect.

Comparison of the O_2- and H_2-associated overvoltages shows that the average overvoltage ΔU_{H_2} is 0.76 V, slightly smaller than the one associated with the O_2 bubbles, $\Delta U_{O_2} = 0.91$ V. In the present work, copper sulphate with Cu II species has been added to avoid the H_2 bubbles evolution for aircraft safety reasons. In fact, a small quantity of hydrogen gas is produced, detectable with CCD cameras under 1G condition, but not under 0G condition.

What is important is the very different behaviour of O_2 and H_2 under zero gravity, as already observed by Fukunaka and Matsushima et al. [1, 2]. During experiments under 0G, videos obtained during parabolic flights show that hydrogen bubbles move far from the cathode instead of O_2 bubbles which stayed attached to the anode. This behaviour difference has also been observed by Prof. Fukunaka [1, 2] with his 0G experiments.

The sum ΔU of these two cell voltage drops has been considered. After bi-linear interpolation, the cell voltage drop associated with both O_2 and H_2 bubbles is

$$\Delta U = 1.67 - 2 \times 10^{-2} Xj - 2.8 \times 10^{-1} XG \quad (9)$$

It appears that for a 30 % current density increase, overvoltage decreases by 4×10^{-2} V, which is about 2 % of the total bubble-associated overvoltage. Concerning the gravity, the absence of the buoyancy forces yields an overvoltage decrease of 0.56 V, which is about 33 %.

From the terminal voltage in both microgravity and in the presence of gravity, it is possible to determine an experimental law for the cell terminal voltage according to the two explored parameters j and G. The empirical law obtained according to the four performed experiments is

$$U_{end} = 3.74 + 1.2 \times 10^{-1} Xj - 2.8 \times 10^{-1} XG \quad (10)$$

The average electrolysis cell voltage for the four experiments is $U_{end} = 3.74$ V and gravity has a more important impact on it than applied current density in the chosen range.

It appears that for a 30 % current density increase, the overvoltage increases by 2.4×10^{-1} V, which is about 6 % of the total cell terminal voltage. In this law, the usual increase of the voltage with applied current density is found again. Concerning the gravity, the absence of the buoyancy forces yields an overvoltage decrease of 0.56 V, which is about 15 %. The last term, associated with experimental dispersion or two explored factors j and G interaction, is so small that this correlation is considered rigorously bi-linear.

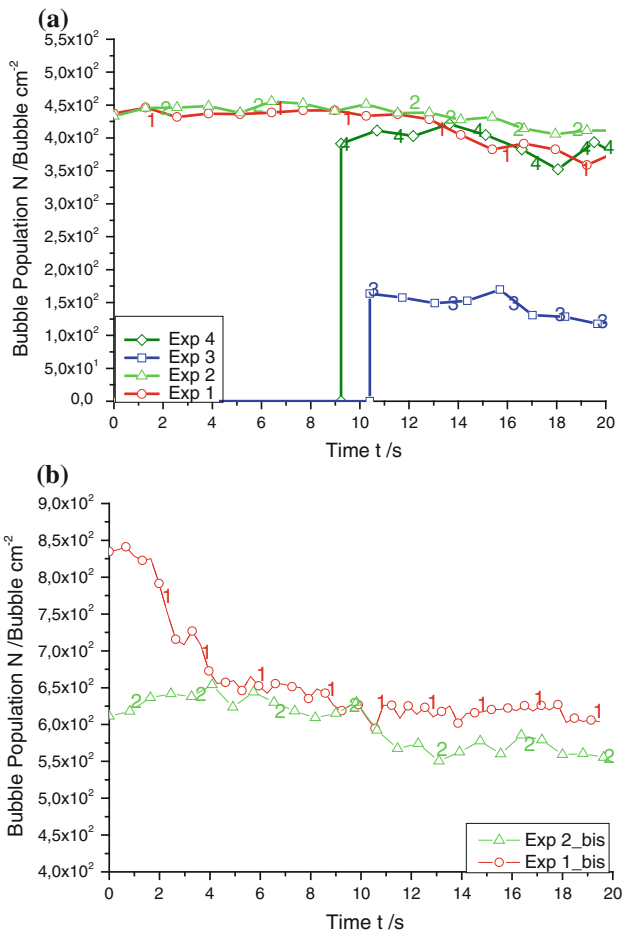

Fig. 8 O_2 (**a**) and H_2 (**b**) bubbles' population N (bubbles cm^{-2}) evolution with time t

Table 6 O_2 and H_2 terminal bubble population N (bubbles cm^{-2})

Exp.	Bubble population N_{O_2}/O_2 bubbles cm^{-2} @ $t = 20$ s	Bubble population N_{H_2}/H_2 bubbles cm^{-2} @ $t = 20$ s
1	$3.8 \times 10^{+2}$	$6.04 \times 10^{+2}$
2	$4.71 \times 10^{+2}$	$5.32 \times 10^{+2}$
3	$1.25 \times 10^{+2}$	×
4	$3.93 \times 10^{+2}$	×

The voltage is larger under normal Earth gravity condition than under zero gravity, although the gas production is the same. It is a clear that the gravity, by affecting the bubble size and population, is of great importance for the electrolysis voltage.

4.2 Bubble diameter, population and void fraction evolution

4.2.1 Bubble diameter evolution

The evolution of the O_2 and H_2 bubble diameters with time is given in Fig. 7a, c, respectively.

In Fig. 7a, it is observed that the O_2 bubble diameter increases with current density and with gravity. Note that O_2 bubbles under $0G$ condition appears after about 10-s electrolysis: This is the time needed to obtain O_2 supersaturation at the anode. Under $1G$ condition, supersaturation conditions are obtained at the end of the first electrolysis. The results shown are those associated with 'bis' experiments. The results show a small dependence of the bubble diameter on the applied current density (Fig. 7a and Table 5): less than 4 %. This confirms what was found in previous work by Vogt [5, 6] and Matshushima [1, 2]. The influence of gravity is three times more important (about 12 %). The diameter increase under $0G$ condition is associated with the absence of the buoyancy force and the induced natural flow.

Figure 7c, associated with H_2 bubbles, shows a different behaviour: The current density effect is about 22 % and no bubbles are detected under $0G$ condition with CCD cameras, though they are produced. The bubbles produced are smaller than the minimal diameter detectable by the camera.

Concerning the standard deviation presented, respectively, for O_2 and H_2 bubbles in Fig. 7b, d, the values are very large, from 67 to 100 % of the average diameter. This means that the bubble diameter distribution is not at all monodisperse and there is a strong dispersion around the average diameter value. This is due to strong coalescence phenomena which occur at both electrodes, but mostly for H_2 bubbles.

After bi-linear interpolation, the O_2 bubble average diameter d_{O_2} (mm) and standard deviation Δd_{O_2} (mm) are

$$O_2 \text{ diameter law: } d_{O_2} = 2.8 \times 10^{-1} + 5 \times 10^{-3} Xj + 1.5 \times 10^{-2} XG \quad (11)$$

$$O_2 \text{ deviation law: } \Delta d_{O_2} = 2.1 \times 10^{-1} + 2 \times 10^{-3} XG - 2 \times 10^{-3} XG + 7 \times 10^{-3}\, Xj * XG \quad (11')$$

It appears that for a 30 % current density increase, the O_2 bubble diameter increases by 10^{-2} mm, which is less than 4 % the average diameter. The diameter standard deviation is not dependent on the applied current density. Concerning the gravity, the absence of the buoyancy forces yields an average O_2 diameter increase of 3×10^{-2} mm, which is three times the current density effect and about 12 % the average diameter. The standard deviation of the diameter is more sensitive to this parameter: With the gravity absence, the standard deviation decreases about 24 %. This means that the interpolation with the two explored factors j and G is not perfectly linear: An experimental dispersion or an interaction should be taken into account, which is much more important, 7×10^{-3} mm, than the two explored factors j and G (1 %).

After linear interpolation, the H_2 bubble average diameter d_{H_2} (mm) and standard deviation Δd_{H_2} (mm) are

$$H_2 \text{ diameter law: } d_{H_2} = 2.55 \times 10^{-1} + 1.5 \times 10^{-2} Xj \quad (12)$$

$$H_2 \text{ deviation law: } \Delta d_{H_2} = 2.5 \times 10^{-1} - 2 \times 10^{-2} Xj \quad (12')$$

It appears that for a 30 % current density increase, the H_2 bubble diameter increase is 3×10^{-2} mm, which is about 12 % of the average diameter; the diameter's standard deviation sensitivity is about the same as the applied current density. There is a larger H_2 bubble diameter distribution when the applied current density increases, whereas the O_2 bubble distribution was not dependent on these explored factors. Note here that the diameter and deviation sensitivity with current density are four times larger for H_2 bubbles than for O_2 bubbles.

Concerning the gravity, it has been noticed during the two experiments 3 and 4 that the CCD cameras could not detect the presence of H_2 bubbles. Nevertheless, a voltage drop associated with this H_2 production is defined.

4.2.2 Bubble population evolution

The evolution of the O_2 and H_2 bubble population, N_{O_2} and N_{H_2} (bubbles cm^{-2}), with time is given in Fig. 8a, b, respectively, and Table 6.

In Fig. 8a, it is observed that the O_2 bubble population increases with current density and decreases with the absence of the gravity. When gravity is absent, for a given current density, the bubbles are less numerous, but with a larger diameter. Under $0G$ condition, it needs about 10-s electrolysis time to obtain O_2 supersaturation at the anode. For a given gravity level G, the O_2 bubbles' diameter and the population increase.

After bi-linear interpolation, the O_2 bubbles' population N_{O_2} (O_2 bubbles cm^{-2}) is

O_2 bubbles' population law:

$$N_{O_2} = 3.42 \times 10^2 + 8.97 \times 10^1 Xj - 8.32 \times 10^1 XG + 4.42 \times 10^1 Xj * XG \quad (13)$$

It appears that for a 30 % current density increase, the O_2 bubble population N_{O_2} increases about 90 bubbles cm^{-2}, which is about 27 % of the initial value. Concerning the gravity, the effect is much stronger with a decrease of 255 O_2 bubbles cm^{-2} under zero gravity.

In Fig. 8b, it is observed that the H_2 bubble population decreases slightly with applied current density, which is contrary of the O_2 bubble behaviour. When gravity is removed, for a given applied current density, the bubbles are not detectable with the used cameras.

After linear interpolation, the H_2 bubble population N_{H_2} (H_2 bubbles cm^{-2}) is

H_2 bubbles population law:

$$N_{H_2} = 5.68 \times 10^2 - 3.6 \times 10^1 Xj \quad (14)$$

It appears that for a 30 % current density increase, the H_2 bubble population N_{H_2} decreases by 7.2×10^1 bubbles cm^{-2}, which is about 13 % of the initial value. Concerning the gravity, the effect is significantly stronger because H_2 bubbles are no longer detectable under zero gravity. During the 20-s experiments, the CCD cameras detect no H_2 bubbles.

In summary, the two-phase layer structure, the bubble diameter and population density are important parameters to explain the cell overvoltage due to bubbles.

4.2.3 Two-phase layers' void fraction

The evolution of the O_2 and H_2 bubbles leads to important boundary layers at both electrodes. The thickness δ and the average gas void fraction ε of both anode and cathode layers lead to an associated overvoltage. The idea of the present work is to associate experimentally defined overvoltages with O_2 and H_2 evolution. We look for the relation between the two-phase boundary layer structures and behaviour (hydrodynamics properties) and the associated overvoltage (electrical property).

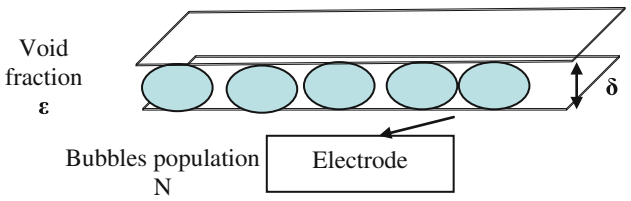

Fig. 9 Electrode two-phase boundary layer structure and gas void fraction ε

It is important to distinguish the two boundary layers at the anode and cathode. According to previous authors' observations [1, 2], the O_2 and H_2 bubble behaviour is quite different for the one explored here. Figure 9 shows a schematic definition of the electrode two-phase boundary layer. The aim is to define correctly this layer structure and its gas void fraction.

The gas void fraction ε has been studied by several authors including Vogt et al. [5, 6], Eighlender et al. [7] and Mandin et al. [8, 9]. The gas void fraction is defined as the ratio

$$\varepsilon = \frac{\text{Totalbubblevolume}}{\text{Total volume}} = \frac{N\pi d^2}{6} \quad (15)$$

where the total volume is the sum of the bubble and liquid volumes in the defined domain.

Because the video recording treatments give us the bubble population N in bubble number per cm^2, we need a layer thickness δ (m) definition to reach one two-phase layer volume definition. This thickness is difficult to experimentally measure: During experiments, some bubbles grow at the electrode edges and the visualisation of the two-phase layer thickness is avoided due to this screening. If the two-phase layer thickness measurement is impossible the determination of the bubble number per cm^2 is still possible. As first hypothesis it is proposed to suppose that the layer thickness is due to one or more generation of bubbles which accumulate at the electrode. For example, only one generation is more appropriate for H_2 bubbles which are detaching from the electrode surface quickly. The thickness δ is supposed to obey $\delta = d$, the bubble diameter (Eq. (14) is written under this hypothesis). Notice that under $0G$, the hydrogen bubbles are not 'seen' with the used CCD camera. Concerning O_2 bubbles, it is more difficult due to their different behaviour compared to the H_2 one. They accumulate and stick to each other to form a multi-generation thick multi-layer. The O_2 bubble size is larger, the dispersion is smaller and the population is less numerous under $0G$ than under $1G$.

In Fig. 10a and Table 7 are presented the evolution with time of the O_2 bubble two-phase boundary layer void fraction ε_{O_2} near the anode for the four defined experiments. Under $1G$ condition, the gas void fraction is about

12 % and seems little dependent on applied current density (8 %). Under 0*G* condition, about 10 s is necessary to observe the bubble appearance with our CCD cameras. We are able to define the gas void fraction only at this time. The bi-linear interpolation for O_2 gas void fraction yields

$$\varepsilon_{O_2} = 1.2 \times 10^{-1} + 2 \times 10^{-2} Xj - 2 \times 10^{-2} XG - 1.5 \times 10^{-2} Xj\,XG \quad (16)$$

The O_2 gas void fraction increases with current density (33 %) and decreases with the disappearance of gravity (33 %). The bi-linear assumption is completed with a last term, the same order of range of the explored factor sensitivity.

In Fig. 10b and Table 7 is presented the evolution with time of the H_2 bubble two-phase boundary layer void fraction ε_{H_2} near the cathode for only two of the four defined experiments. This is due to the non-appearance of H_2 bubbles in CCD recordings during 20-s electrolysis under 0*G*. Under 1*G* condition, the gas void fraction is about 20 % and seems little dependent on the applied current density (10 %). Notice that the gas void fraction seems to be, for a long time, smaller for the larger current density, except at the end (@ $t = 20$ s). Because of the

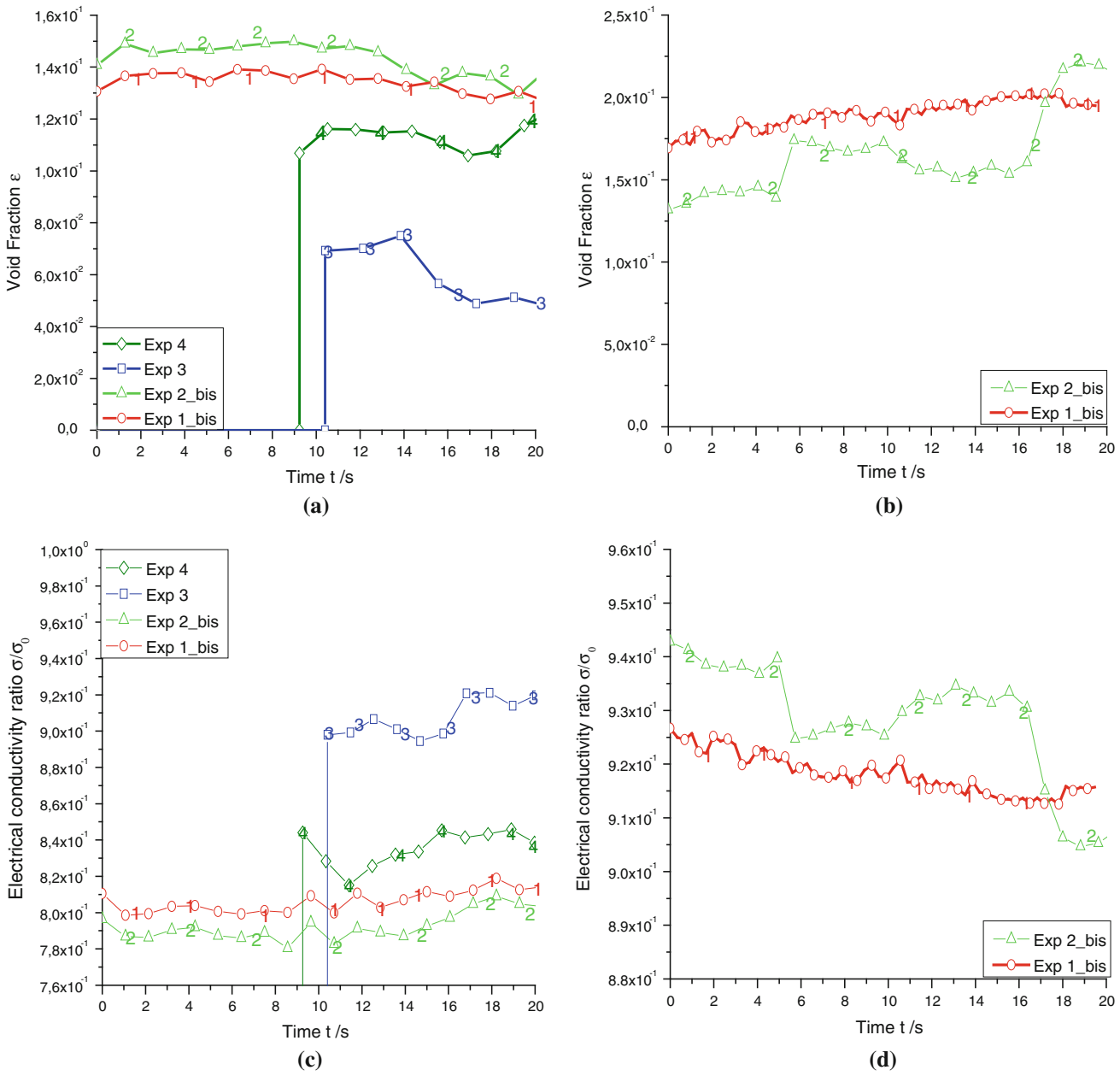

Fig. 10 Two-phase layer void fraction ε (−) for O_2 (**a**) and H_2 (**b**) and conductivity ratio σ/σ_0 (−) for O_2 (**c**) and H_2 (**d**) evolution with time *t*

larger current density value, one can think of larger gas bubble production according to Faraday's law. One can imagine that a larger bubble population N is attached to the electrode. The bubble diameter d increases with current density, whereas the bubble population N increases for O_2 and decreases for H_2 with current density j. At the end, it is difficult to clearly explain the gas void fraction ε evolution with current density j, in the present case an increase for both O_2 and H_2.

The linear interpolation for ε_{H_2} yields

$$H_2 \text{ void fraction law: } \varepsilon_{H_2} = 2 \times 10^{-1} + 1 \times 10^{-2} Xj \quad (17)$$

The H_2 gas void fraction increases slightly with current density (10 %).

The gas void fraction is integrated in the equivalent electrical conductivity and the resulting voltage drop calculation is given in next section.

4.3 Two-phase layer equivalent electrical conductivity

For two-phase thin layers, with a gas volume fraction ε (the gas is supposed to have no electrical conductivity), the Bruggeman law gives the equivalent electrical conductivity σ:

$$\sigma = \sigma_0(1 - \varepsilon)1.5 \quad (18)$$

Where σ_0 = 3.42 S m^{-1}, is the liquid electrolyte electrical conductivity (with no bubbles, Table 1) and ε the thin layer void fraction.

Figure 10c, d and Table 7 give the two layer equivalent electrical conductivity ratio σ/σ_0 according to the gas void fraction evolution given in Fig. 10a, b. The changes are larger under $1G$ condition than under $0G$ condition. Because the O_2 bubbles are larger, the gas void fraction is smaller and the electrical conductivity ratio is larger. The current density j effect is larger for the O_2 layer than for the H_2 layer, according to the experimental interpolation performed:

O_2 layer equivalent electrical conductivity ratio law:

$$\sigma_{O_2}/\sigma_0 = 8.4 \times 10^{-1} - 2 \times 10^{-2} Xj + 3.5 \times 10^{-2} XG - 1.5 \times 10^{-2} Xj\, XG \quad (19)$$

H_2 Layer equivalent electrical conductivity ratio law:

$$\sigma_{H_2}/\sigma_0 = 9.1 \times 10^{-1} - 5 \times 10^{-3} Xj \quad (20)$$

The presence of a two-phase layer yields an average change in the 'near electrode' electrical conductivity of about 16 % less for the O_2 layer and 9 % less for the H_2 layer.

The current density importance is nevertheless small with about 4 % for the O_2 layer and 1 % for the H_2 layer. The importance of the gravity disappearance on the O_2 electrical conductivity is larger, about 7 %.

4.4 Two-phase layer voltage drop

For both two-phase thin layers at the anode and cathode, there is an equivalent electrical conductivity σ decrease which leads to a surface voltage drop that we are interested in for our electrochemical engineering process modelling application.

In a one-dimension, purely diffusive media (Ohm hypothesis), one can consider the simple serial resistance modelling for cell voltage calculation. This hypothesis neglects the migration and convection transport. The migration can be neglected in our case due to the large electrical conductivity (σ_0 = 3.42 S m^{-1}). The convection transport can be rigorously neglected under $0G$ condition, but not under $1G$ condition. A first model is shortly presented here. A more advanced model using numerical multi-physics modelling and Computational Fluid Dynamics will be presented in a further communication.

Under 1D geometry hypothesis, the cell voltage drop due to bubbles is modelled according to Eq. (21):

$$\Delta U = \delta * j/\sigma \quad (21)$$

where δ (m) is the two-phase boundary layer thickness, j (A m^{-2}) the applied current density and σ (S m^{-1}) the layer equivalent electrical conductivity. The lesser known parameters among them are δ and σ. The first is estimated as one or more times the steady average bubble diameter (which is a non-measured hypothesis). The second is estimated with the help of the Bruggeman theory.

Table 8 gives a final view of the present work. The two last rows are dedicated to the previously given (Table 3) voltage drops associated with both O_2 and H_2 bubble appearances. This table also gives the theoretical voltage drops calculated with a simple 1D resistance model. The present strategy is interesting because a link is established between voltage drops, which have been defined with potentiostat measurements, and CCD recordings in term of bubble size and population. The link between electrical and video measurements is possible using a set of hypothesis: 1D resistance modelling, no convection and migration,

Table 7 O_2 and H_2 two-phase layer void fraction ε (−) and equivalent electrical conductivity σ/σ_0 (−)

Exp.	ε_{O_2} @ t = 20 s	ε_{H_2} @ t = 20 s	σ_{O_2}/σ_0 @ t = 20 s	$\varepsilon_{H_2}/\sigma_0$ @ t = 20 s
1	1.2×10^{-1}	1.9×10^{-1}	8.1×10^{-1}	9.1×10^{-1}
2	1.3×10^{-1}	2.1×10^{-1}	8×10^{-1}	9×10^{-1}
3	4.7×10^{-2}		9.1×10^{-1}	
4	1.2×10^{-1}		8.4×10^{-1}	

Table 8 Theoretical 1D and experimental voltage drops ΔU (according with Table 4) associated with both O_2 and H_2 layers at electrodes

Exp.	ΔU_{O_2} theoretical (V)	ΔU_{H_2} theoretical (V)	ΔU_{O_2} (V) @ $t = 20$ s	ΔU_{H_2} (V) @ $t = 20$ s
1	3.08×10^{-2}	2.53×10^{-2}	1.28	6.9×10^{-1}
2	4.35×10^{-2}	3.87×10^{-2}	1.16	7.7×10^{-1}
3	3.06×10^{-2}	X	6×10^{-1}	8.1×10^{-1}
4	4.45×10^{-2}	X	5.9×10^{-1}	7.8×10^{-1}

considered layers thickness equal to one bubble average diameter and Bruggeman theory for the dynamic two-phase layers. Nevertheless, these simple hypotheses are limited. As can be seen, the voltage drop differences between the (video + 1D modelling) and the direct potentiostat measurements are quite large. The modelled voltage drop for O_2 only represents 2.4 % of the experimentally measured voltage drop under the experiment 1 condition; only 3.7 % for the H_2 one. The sensitivity with the applied current density is also poorly described: For O_2 and H_2, an overvoltage increase is predicted for a current density increase, though potentiostat measurements show a decrease. Concerning overvoltage sensitivity with gravity, it has been only obtained for O_2 as H_2 bubbles were not visible with the CCD. The 1D theoretical model shows little dependence to gravity, whereas the gravity influence on the potentiostat-measured voltage drops are large. The O_2-associated voltage drop is only half the normal Earth gravity under zero gravity condition, mostly due to, for a given current density, the two-phase boundary layer structure modification, the change in diameter and the convection disappearance.

5 Conclusions

Experiments have shown a significant sensitivity of the voltage drops, bubble diameter distribution, bubble population, gas void fraction and electrical conductivity, with the explored factors current density and especially gravity. This demonstrates the great interest of zero gravity experiments.

H_2 and O_2 bubbles do not have the same behaviour: H_2 bubbles leave the cathode after a short time, whereas O_2 bubbles stick and accumulate at the anode. Among all the bubbles produced per unit time, one part adheres at the electrode, the other leaves. In the case of H_2, the leaving part is larger, whereas for O_2 bubbles, the adhering part is larger.

The main conclusion here is to see the necessity, for an accurate and realistic two-phase process modelling, of a multi-physics modelling and a rigorous description of two-phase hydrodynamic properties and their consequences on both two-phase layers at the anode and cathode. Simple 1D resistance modelling is not sufficient for such non-linear, non-Ohm conductive media. Future, more accurate modelling, of such two-phase electrolysis might include some dedicated description of phenomena such as

- Surface screening θ due to bubbles adhering at electrodes;
- Actual current density at the electrode (taking into account the bubble screening θ) ;
- Actual activation overvoltage at electrodes according to the Buttler-Volmer laws;
- Actual gas void fraction;
- Actual mass transfer enhancement at electrodes due to the bubbles motion;

All these points are to be explored to ensure the correct modelling of such two-phase electrolysis processes.

Acknowledgments The authors wish to thank French ANR AMELHYFLAM, CNES, ESA, Brittany Region, BGS® and Novespace® for their help and support. Also, our warm thanks to Michel Dumons, Jean Costa, Frederic Mesguen, Gilles Piat, Adrien Fuentes, Thomas Pierre, Thibault Colinart, Brigitte Lignot, Alain Fuchs, Bernard Zappoli, Yannick Bailhé, Adeline Robb, Gérémy Boyer, professors Johan Deconinck, Philippe Viers and Laszlo Kiss and all involved students and persons from Lorient South Brittany University and Technology Institute.

References

1. Matsushima H, Nishida T, Konishi Y, Fukunaka Y, Ito Y, Kuribayashi K (2003) Electrochim Acta 48:4119–4125
2. Matsushima H, Fukunaka Y, Kuribayashi K (2006) Electrochim Acta 51:4190–4198
3. Brussieux C, Viers Ph, Roustan H, Rakib M (2011) Electrochim Acta 56:7194–7201
4. Derhoumi Z, Mandin Ph, Wuthrich R, Roustan H (2011) J Appl Fluid Mech 4:81–87
5. Vogt H, Aras Ö, Balzer RJ (2004) Int J Heat Mass Transf 47:787–795
6. Vogt H, Balzer RJ (2005) Electrochim Acta 50:2073–2079
7. Eigeldinger J, Vogt H (2000) Electrochim Acta 45:4449–4456
8. Mandin Ph, Hamburger J, Bessou S, Picard G (2005) Electrochim Acta 51:1140–1156
9. Mandin Ph, Roustan H, Wüthrich R, Hamburger J, Picard G (2007) Transactions on engineering sciences. WIT Press, p 73
10. Wüthrich R, Comninellis Ch, Bleuler H (2005) Electrochim Acta 50:5242–5246
11. Wüthrich R, Hof LA, Lal A, Fujisaki K, Bleuler H, Mandin Ph, Picard G (2005) J Micromech Microeng 15:268
12. Dukovic J, Tobias CW (1987) J Electrochem Soc 134:331–343
13. Guo H, Zhao JF, Ye F, Wu F, Lv CP, Ma CF (2008) Microgravity Sci Technol 20:265
14. Kiuchi D, Matsushima H, Fukunaka Y, Kuribayashi K (2006) J Electrochem Soc 153:E138
15. Kaneko H, Tanaka K, Iwasaki A, Abe Y, Negishi A, Kamimoto M (1993) Electrochim Acta 38:729
16. Iwasaki A, Kaneko H, Abe Y, Kamimoto M (1998) Electrochim Acta 43:509
17. Nicolau E, Poventud Estrada CM, Arroyo L, Fonseca J, Flynn M, Cabrera CR (2012) Electrochim Acta 75:88